Manganese ferrite nanoparticle production from industrial wastes as sorbent material for arsenic removal from aqueous solutions

Ünzile Yenial[1,2], Gülay Bulut[1], Francesca Pagnanelli[2]

[1]Istanbul Technical University, Mineral Processing Engineering Department, 34469, Istanbul Turkey

[2] Sapienza University of Roma, Chemistry Department, Piazzale Aldo Moro 5, 00185 Roma Italy

Contact: yenial@itu.edu.tr

ABSTRACT

Manganese ferrite nanoparticles were prepared by microwave-sonication assisted hydrothermal route and produced from wastes of Li-ion batteries and pyrite ash. The leaching solution of waste pyrite ash was used for Fe source while, Mn-bearing solution recovered from the recycling process of end life Li-ion batteries was used as Mn source. X-ray diffractometry evidenced that manganese ferrite can be obtained as single crystalline phase. Scanning Electron Microscope images showed that double-pyramid or octahedron particles were formed with the average size of 24.3 nm. This produced $MnFe_2O_4$ nanoparticles denoted good sorption capacity towards to As (101±0.5 mg/g at pH 3).

Keywords: manganese ferrite; nanoparticles; adsorption; arsenic; hydrothermal synthesis; Li-ion batteries

1. INTRODUCTION

Nanoparticles represent one of the most important progress in different technological applications such as catalysis, photonics, and electronics due to dramatic changes induced by size reduction (Naseri, Saion, and Shaar, 2012). Nanoparticles have received extensive attentions in the field of pollutant adsorption and environmental remediation due to their adsorbing and magnetic capabilities, and the main advantages of using nanoferrites as sorbent materials rely on the high specific surface area associated to low size particles, and on the easiness of separation of exhausted solids by the application of magnetic fields.

Magnetic nanoparticles of transition of metal ferrite nanoparticles having spinel structure are great of interest for their properties, having super paramagnetic behavior (Carta et al. 2010). Over the past years spinel ferrite nanoparticles have taken considerable attention due to soft magnetic properties (low coercivity, moderate saturation magnetization) (Goldman 1993). Manganese ferrite, $MnFe_2O_4$, also belongs to a group of soft magnetic materials ($Hc < 10$ A/Cm) characterized by high magnetic permeability, low losses, high saturation magnetization (Ms) and relatively high Curie temperature (Vijaya, Sekaran, and Bououdina, 2015). Manganese ferrite is a magnetic ferrite with cubic spinel structure, which has been used in various technological applications (magnetic materials, gas sensor, and absorbent material for hot gas) (Sharma, Sharma, and Shah, 2014). Nanosized manganese ferrite was stated to be a promising material for environmental applications, as adsorbent material for different inorganic and organic pollutants (Stoia, Muntean, and Militaru, 2015).

Several methods have been applied to produce Mn-ferrite nanoparticles such as sol-gel (Atif Hasanain, and Nadeem, 2006) mechanical ball-milling technique (Jiang et al. 1999), coprecipitation (Shenoy et al., 2004) polymeric-assisted route (Zhang et al. 2010), the hydrothermal method (Atia et al. 2016), the reverse micelles process (Kale, Gubbala, and

Misra, 2004) and the microemulsion method (Hochepied, Bonville, and Pileni, 2000). Most of these methods have achieved particles of the required sizes and shapes, but they are difficult to employ on a large scale because of their expensive and complicated procedures, high reaction temperatures, long reaction times, toxic reagents and by-products, and their potential harm to the environment (Naseri et al. 2011).

In the literature there are several papers about $MnFe_2O_4$ synthesizing with coprecipitation and some modified methods. Naseri et al. (2011) produced manganese ferrite nanoparticles by a thermal treatment method following calcination. They used polyvinyl pyrrolidon (PVP) as a surfactant to control the agglomeration of the nanoparticles. The smallest particle size of the material was observed as 12 nm. Bhowmik et al. (2016) also produced manganese ferrites by coprecipitation route by adding NaOH as pH modifier. They obtained nanoparticles in a mixed phase of crystalline $MnFe_2O_4$ and Mn_3O_4 with excellent magnetic properties and with high specific surface area (100.62 m^2/g). They successfully removed the methyl orange dye from water by adsorption method. Sezgin et al. (2013) studied the removal of copper, zinc and nickel from synthetic waste water using nanoparticles. The $CuFe_2O_4$ and $NiFe_2O_4$ nanoparticles were produced with surfactant assisted hydrothermal method. The removal efficiencies of Cu(II), Ni(II) and Zn(II) with $CuFe_2O_4$ nanoparticles were calculated as 83.50%, 98.85%, and 99.80%, respectively. The removal efficiencies of Cu(II), Ni(II), and Zn(II) with $NiFe_2O_4$ nanoparticles were calculated as 92.55%, 36.56 %, and 99.91%, respectively. Arsenic removal was investigated with mesoporous magnetic $MnFe_2O_4$ (Hu et al. 2017). However there is no enough information about arsenate adsorption onto manganese ferrite nanoparticles.

Generally metal salts are being used for synthesizing manganese ferrite nanoparticles in the literature, and there are only a few studies dealing with wastes. The preparation of manganese ferrite from industrial wastes and impure metal solutions is a novel procedure aiming at

valorizing metal-bearing wastes and simultaneously removing metal pollutants from wastewater (Rashad et al. 2012). Metal containing wastes or byproducts can be utilized for new material synthesizing. The processing of metal containing wastes and recovery of valuable components and in some cases converting them into useful compounds/materials is the best environmental solution (Rao 2006). Especially mining/ metallurgical processing wastes constitute high amount of wastes in Turkey. The total 26 million tons of tailings have been discarded as waste from mineral processing plants. These wastes are generally landfilled or dumped, and in some cases it causes serious land and environmental pollution problems due to the release of toxic substances (Alp et al. 2008).

The coprecipitation method, which is a simple method to produce spinel nanoparticles, is also advantageous for purification of metal bearing waste solutions. Therefore in this work, production of manganese ferrite nanoparticles from industrial wastes with coprecipitation method using Mn-bearing solution (from lithium ion battery process) (Pagnanelli et al. 2016) and Fe-bearing solution (pyrite ash of sulfuric acid production plant) was studied. For this aim different parameters were tested in order to synthesize magnetic, small sized, stabile nanoparticle. The best product was used as adsorbing material to remove arsenic from synthetic solutions; the parameters as pH, contact time and initial concentrations were investigated.

2. MATERIAL AND METHOD

All the experiments were performed with analytical grade of reagents and metal sulfate solutions prepared as explained below. H_2SO_4 for leaching agent was received from Sigma Aldrich, polyvinyl pyrrolidon (PVP) (MW= 10000) from Sigma Aldrich was used as surfactant to control the agglomeration of particles, NaOH as precipitation agent and pH

modifier (Sigma Aldrich), methanol from Sigma Aldrich in washing treatment to remove excessive amount of , HCl as pH modifier (Sigma Aldrich).

2.1 Material

The materials pyrite ash (Yenial et al. 2016) and Li-ion batteries (Granata et al. 2012) were the main industrial wastes used in this study. Pyrite ash was obtained from sulfuric acid production plant which is located in Bandırma, Turkey. Bandırma sulfuric acid production factory has 95000 ton/year technical and 25000 ton/year pure, annual sulfuric acid production capacity. In this factory, sulfuric acid was produced by contact method with using flotation pyrite. Pyrite ashes were obtained like wastes from roasting of pyrite ores to produce sulfuric acid. This waste was a byproduct of pyrite incineration to produce sulfuric acid and mainly contained iron oxides, silicates and some unburned pyrites (Alp et al. 2008). The Fe-bearing solution was produced by leaching pyrite ash with 3M H_2SO_4 in microwave digester (Ethos 900) for 2h and 200°C with 1/10 solid liquid ratio. The analysis of this solution is given in Table 1.

The other waste material Li-ion batteries were collected by S.E.Val. s.r.l. (Italy) first crushed and then ground for leaching processes. This electrodic powder was leached by adding H_2O_2 and H_2SO_4. After leaching, precipitation was applied for removal of iron, and after solvent extraction was applied to separate manganese from liquor. Mn-bearing organic phase was stripped with sulfuric acid and Mn-bearing solution that was used as Mn source in the experiments. The flowsheet of this procedure is given in Figure 1 (Pagnanelli et al. 2016). The chemical analysis of Mn-stripping solution is shown in Table 1.

Figure 1.

Table 1.

2.2 Methods

The methods for nanoparticle synthesis, adsorption and analyzing methods were explained in below.

2.2.1 Nanoparticle Synthesis Method

Manganese ferrite nanoparticles were synthesized upon the method of ultrasonic wave and surfactant assisted hydrothermal synthesis (Atia et al. 2016). Hydrogen peroxide was added to oxidize Fe^{2+} to Fe^{3+} in Fe-leaching solution. The Mn-stripping solution and Fe-leaching solution mixed in the molar ratio of Fe^{3+} and Mn^{2+} 2:1. Under vigorous stirring, nonionic surfactant PVP (polyvinyl pyrolidine) was added to the solution in the same molar ratio of Fe^{3+}. The pH of the solution was constantly monitored as the 5M NaOH solution was added. The sonication was applied while the pH of the solution was increased to pH 12.5 and black precipitate was obtained. After 10 min sonication, the solution was mixed for 2 hours at 60°C, using magnetic stirrer. The precipitate was left for 30 min for sedimentation; the condensed part was separated from solution and placed in microwave digester for 2 h at 200°C. Subsequently, the precipitate was washed five times with distilled water and once with methanol to remove excessive amount of sodium hydroxide and organic. The residual organic and sodium concentrations were determined upon EDX analysis. The nanoparticle containing solution was centrifuged for fifteen minutes at 3000 rpm to isolate the supernatant liquid. The precipitate was dried in oven for 24 h at 105°C.

The effect of PVP surfactant amount and microwave thermal treatment on Mn-ferrite nanoparticle production was investigated with four different experiments. The experimental

conditions were shown in Table 2, the molarity of PVP agent and the application of thermal treatment were tested. The molar ratio of Fe and Mn should be 2:1 due to stoichiometric ratio, but in these experiments, it was used over than the ratio, because leach solutions contain not only Mn, but also other metals such as Co, Cu and Zn. The results were evaluated with particle size and SEM images.

Table 2.

2.2.2 Adsorption Experiments

The adsorption experiments were carried out at ambient temperature to test the adsorbing capacity of the manganese nanoparticles towards to arsenic ion. The effect of contact time, initial As concentrations and pH were investigated. The experiments were conducted by suspending nanoparticles (0.25 g/L) in 1mM As solution using an orbital shaker (New Brunswick Scientific G25 Incubator Shaker, 140 rpm) at room temperature. The contact time experiments were conducted from 2 to 24 h. The pH effect was investigated at different pH's as 3.3, 3.75, 5.0, 6.25, 7.2, 9.6, 11.6. The metal removal capacity was determined with different initial concentrations from 11 mg/L to 150 mg/L.

Arsenic concentration in solid phase (Qm, mg/g) was estimated by metal mass balance in the system by the following equation:

$$Qm= (Ci-Cf)* V/M \quad (1)$$

Where Ci (mg/L) is the initial adsorbate concentration in the solution, Cf (mg/L) is the adsorbate concentration in the solution at equilibrium, V (L) is solution volume and M is adsorbent amount (g).

2.2.3 Analytical procedures

The chemical analysis (Al, Ca, Cu, Co, Fe, Mn, Ni, Zn) of the samples was done with Atomic Absorption Spectrometry (Jena 300). The detection limit of Zn is 0.0273 mg/L; Fe is 0.0381 mg/L; Mn is 0.0226 mg/L; Cu is 0.0031 mg/L. The micro structure and surface morphology of the samples have been examined using HR FESEM Zeiss Auriga field emission scanning electron microscopy (FE-SEM) and energy dispersive X-ray spectroscopy (EDX). The particle size of the nanoparticles are calculated with open access Image J program, the average sizes of the nanoparticles were calculated on 100 nanoparticle measurements. XRD patterns have been provided by Rigaku D-max and interpreted with Match! XRD calculation program. The specific surface area was determined by the gas adsorption method developed by Brunauer, Emmett and Teller (BET), using a Micromeritics 3Flex 3.01. The samples were pre-treated under vacuum at 180°C for 2 hours. The BET specific surface area of manganese ferrite nanoparticle was found as 158.6±0.3 m^2/g, with total pore volume of 0.217 cm^3/g. Fourier transform infrared spectroscopy (FT-IR) spectra were recorded on a PerkinElmer spectrum FT-IR using KBr pellets. The magnetic properties of the nanoparticles were measured with the Physical Properties Measurement System magnetometer at 298 K (Quantum Design, USA). The magnetization measurement was taken from the −70 kOe to 70 kOe field. The saturation magnetization (M_s) was determined from the magnetization vs applied field curve.

In addition a hand magnet was used to determine nonmagnetic-magnetic samples and removal of used magnetic Mn-ferrite nanoparticles from solution after adsorption. The residual arsenic concentrations were analyzed with UV-spectrophotometer with photometric ammonium molybdate method (detection limit: 0.02 mg/L).

3. RESULTS AND DISCUSSION

3.1 Characterization of $MnFe_2O_4$ Nanoparticles

3.1.1 Particle Size and Morphology Studies

Figures 2, 3, 4 and 5 shows the nano-structured materials morphology, which changes with the parameters such as surfactant (PVP) amount and microwave energy.

Figure 2 shows the SEM imagining of the sample which is produced without microwave thermal treatment. This sample is dried in oven for 24 h at 105°C after precipitation. The nanoparticles displayed a rough surface without any particle shape or crystals occurred and found as non-magnetic. Figure 3 shows SEM image of the sample that was produced in microwave without PVP. The material was amorphous and flower-like, therefore the particle size was not determined and found as non-magnetic. The high yield of $MnFe_2O_4$ nanoparticle production depended on concentration of surfactant, with desired ratio of Mn and Fe. This was because, during the microwave combustion, the precursors were adsorbed onto preferred planes and changed the growth kinetics (Vijaya, Sekaran and Bououdina, 2015). Therefore in the nucleation stage without surfactant, resulted the flower-like amorphous morphology. In the literature flower-like shape was defined for δ-MnO_2, which were microsized and comprise a large number of thin nanosheets (Duan et al. 2012). When the concentration of PVP increased the morphology changed as octahedron (Figure 4 and 5). Figure 4a shows the SEM imagining of the sample produced in the different molar ratio of Fe and PVP (2:1). The nanoparticles had bi-pyramid or octahedron shape but not uniform and in some places it was not well crystallized. Figure 4b shows the particle size distribution of this material. The average size of the nanoparticles was found as 66.3 nm. These nanoparticles were found to be magnetic. Figure 5a shows the SEM image of the $MnFe_2O_4$ produced with the conditions of equal molarity of PVP and Fe (1:1) with the presence of microwave energy. The synthesized manganese ferrite nanoparticles were mostly bi-pyramid or octahedron and sporadically truncated octahedron. The particle size distribution is shown in Figure 5b, and found that the average particle size as 24.2 nm while the smallest nanoparticle had 8.9 nm size. This material

was determined as magnetic. Hence, it was concluded that the morphology of $MnFe_2O_4$ sample changed gradually from amorphous to nano-flower like and then to octahedron with the increase in PVP ratio. The presence of PVP and application of microwave energy affected the crystal shape and magnetic behavior of the $MnFe_2O_4$. The samples S2, S3 and S4 showed the result of PVP/Fe ratio added in proportion of 0, 0.5 and 1. The PVP played important roles to synthesize manganese ferrite nanoparticles, by controlling the size of nanoparticles and agglomeration increasing the crystallinity of the nanoparticles and having uniform shapes distribution (Naseri, Saion, and Shaar, 2012). The samples S1 and S4 showed the microwave energy application on nanoparticle growing. Microwave energy was found effective in crystal shape and growth which produced enormous amount of heat and sudden combustion process, therefore accelerated nucleation growth (Naseri et al. 2011)

EDX spectrum of produced manganese ferrite nanoparticle (S4) revealed the presence of iron, manganese, copper, zinc, oxygen, carbon (traces of PVP), silicon (due to the specimen used for analysis). In Figure 6, an example of EDX spectrum was reported for sample S4. The relative abundance of elements of the sample confirmed the stoichiometric ratio between Fe/Metals 2.1. The presence of Cu, Zn and Al was originated from Mn-bearing solution.

Figure 2.

Figure 3.

Figure 4a. Figure 4b.

Figure 5 a: Figure 5b:

Figure 6.

3.1.2 Magnetic Properties

Magnetic properties of the Mn-ferrite nanoparticles were determined at room temperature in the applied magnetic field from -70 to 70 KOe. Figure 7 displayed magnetic hysteresis loops of Mn-ferrite nanoparticles. It could be seen that Mn-ferrite nanoparticles demonstrated paramagnetic nature. The values of saturation magnetization (Ms), coercivity (Hc) and remanence (Mr) of Mn-ferrite nanoparticles was measured as 37.25 emu/g, 87.4 Oe and 4.23 emu/g, respectively. The low remanence and coercivity indicated the paramagnetism of these magnetic nanoparticles (Zhang et al. 2010).

Figure 7.

3.1.3 X-Ray Diffraction (XRD) Analysis

The formation of manganese ferrite nanoparticles was investigated by X-Ray Diffraction analysis. Figure 8 shows the XRD plot between Bragg's angle 2θ and the intensity of X-ray. The major characteristic peak (311) and the others peaks (111) (202), (400), (313), (422), (333) and (404) which confirm the presence of single phase of $MnFe_2O_4$ with face centered cubic structure. The structural model was taken as the spinel phase with the space group Fd3m.

Lattice parameters for the spinel phase were calculated using the formula;

$$a = d\sqrt{(h^2 + k^2 + l^2)} \qquad (2)$$

where, ‘a’ is lattice constant (Å), ‘d’ is inter planar distance; h, k, l are the Miller indices of the crystal planes and found as 8.371 Å. The average crystallite size was calculated using Scherer’s relation,

$$D = \frac{0.9\lambda}{\beta \cos\theta} \text{ nm} \quad (3)$$

where, D is the average crystallite size, β is the full width at half maximum for the major peak (311), λ is the X-ray wavelength and θ is the Bragg angle. Average crystallite grain size (D) is found as 22.94 nm which is in good agreement with SEM measurements (Figure 4a, 4b).

Figure 8.

3.1.4 FT-IR Analysis

Figure 9 shows the FT-IR spectrum of $MnFe_2O_4$ magnetic nanoparticles in the range between 400 and 4000 cm^{-1}. The absorption band appeared at 3399 cm^{-1} which is characteristic stretching vibration of hydroxyl functional group (H-O-H) on the surface of nanoparticles or adsorbed water in the sample. The bending vibration of hydroxyl group also detected at 1629 cm^{-1} (Xia et al., 2015). The peak at 1385 cm^{-1} is assigned to vibrations of C=C and other peak at 1125 cm^{-1} can be attributed to the vibrations of –CH induced from PVP. Generally, the metal oxide vibrations occur under 1000 cm^{-1} which is a common character of ferrites (Zipare et al. 2015). The two peaks at 580 cm^{-1} and 435 cm^{-1} correspond to intrinsic stretching vibrations of (Fe-O) which are indicative of formation of spinel ferrite structure. As can be seen from the spectra, the normal mode of vibration of tetrahedral cluster (580 cm^{-1}) is higher than that of octahedral cluster (435 cm^{-1}).

Figure 9.

3.2 DISSOLUTION TESTS

The dissolution tests of metal contained in ferrite nanoparticles (Mn, Fe, Zn, and Cu) were performed in order to assess the operative range of application of these sorbent materials, i.e. the pH for which no metal secondary release was observed. The results are shown in Table 3. According to pH, high amount of Mn release was observed from pH 2 to 4.7 which was in probably due to the presence of secondary phase of Mn oxide. Iron dissolution occurred only under pH 3 is evidencing that the ferrite structure is stable for larger pH than pH 3. Low amounts of Cu and Zn were derived from metal oxides within ferrite structure. Therefore when the solution pH is over pH 5.6, the metal releases were lower than 1 mg/L. The low metal release would not cause metal pollution in aquatic media, indication good stability of the manganese ferrite nanoparticles.

Table 3.

3.3 ADSORPTION TESTS

3.3.1 Determination of Contact Time

In order to determine the optimum contact time to be sure the adsorption/desorption are achieved to equilibrium, from 2 to 24 hours adsorption tests were applied at pH 3, and the results are shown in Figure 10. According to the test, it is found that increasing contact time was increased the adsorption amount of arsenic from 67.07 mg/g to 101 mg/g and 6 hours contact time is enough to achieve equilibrium between arsenic ion and Mn-ferrite nanoparticles.

Figure 10.

3.3.2 Effect of pH

The experimental conditions were 89.1 mg/L (1 mM) As concentration, 2 h contact time and ambient temperature. The results of arsenic adsorption at different pH's were showed on Figure 11. The arsenic adsorption was clearly dependent on pH and decreasing pH increased the arsenic adsorption on manganese ferrite nanoparticles. This result is caused from two factors which is arsenic speciation depending on pH and surface charge of nanoparticles that designates attraction or repulsion between adsorbent surface and adsorbate. The dominant species are $H_2AsO_4^-$ from pH 2 to 7, $HAsO_4^{2-}$, from pH 7 to 11.8 and AsO_4^{3-} from pH 11.8 to 14. For acidic pH arsenic is present as anion in solution, while active sites onto nanoferrites are positively charged thus As adsorption is favored in acidic conditions (Zhang et al. 2010). According to these findings, the highest arsenic adsorption (67.07 mg/g) was observed at pH 3, and following test was applied at this pH.

Figure 11.

3.3.3 Equilibrium sorption tests

In order to determine sorption capacity of Mn-ferrite nanoparticles in equilibrium time at pH 3, different initial As concentration were tested such from 11 mg/L to 150 mg/L. The final As concentration against to adsorbed amount on nanoparticles is shown in Figure 12. According to the test, it is found that increasing initial arsenic concentration showed that the maximum adsorbing capacity of Mn ferrite nanoparticles is 101±0.5 mg/g. The residual As concentration in the solution was found as 0.78 mg/L which is under wastewaters limits (10 mg/L).

Figure 12.

4. CONCLUSION

Magnetic $MnFe_2O_4$ nanoparticle was successfully synthesized by ultrasonic wave and surfactant assisted hydrothermal synthesis from industrial wastes. On this basis, the leaching solution of waste pyrite ash and Li-ion batteries were used as Fe and Mn sources. The results of SEM analysis indicated that the nanoparticles had 24.2 nm size with octahedron shape. The XRD analysis showed there is $MnFe_2O_4$ single crystal. The obtained manganese ferrite nanoparticles were used as adsorbents to remove arsenic from solutions. The maximum adsorption capacity was found as 101±0.5 mg/g and favored at acidic pH.

The proposed synthesizing method of $MnFe_2O_4$ from waste materials for treatment of arsenic containing waste solutions represents an environmental cycle. The production of magnetic nanomaterial from different metals containing solutions helps purification of the leaching solutions. Moreover the treatment of waste water by adsorbing target ion onto magnetic nanomaterial and removing them from solution by an external magnetic source promotes to clear waste water streams. Therefore the present study may serve a reference work and the research outcomes can be applied for designing of production magnetic nanoparticles and treatment arsenic containing waste water streams.

Compliance with ethical standards

Conflict of interest

Author Ünzile Yenial has recieved research grant from Scientific and Technological Research Council of Turkey (TUBITAK) BIDEB 2214-A Doctoral Scholarship program. Other authors declare that they have no conflict of interest.

REFERENCES

Alp, I., Deveci, H., Yazıcı, E.Y., Türk, T., Süngün. Y.H., 2009. Potential use of pyrite cinders as raw material in cement production: Results of industrial scale trial operations, J. Hazard. Mater. 166, 144-149.

Atia, T.A., Altimari, P., Moscardini, E., Pettiti, I., Toro, L., Pagnanelli, F., 2016. Synthesis and Characterization of Copper Ferrite Magnetic Nanoparticles by Hydrothermal Route. Chem. Eng. Trans. 47, 151-156.

Atif, M., Hasanain, S.K., Nadeem, M., 2006. Magnetization of sol-gel prepared zinc ferrite nanoparticles: effects of inversion and particle size. Solid. State. Commun. 138, 416–421.

Bhowmik, L., Debnath, A., Nath, R.K., Das S., Chattopadhyay, K.K., Saha B., 2016. Synthesis and characterization of mixed phase manganese ferrite and hausmannite magnetic nanoparticle as potential adsorbent for methyl orange from aqueous media: Artificial neural network modeling. J. Mol. Liq. 219, 1010–1022.

Carta, D., Casula, M.F., Floris, P., Falqui, A., Mountjoy, G., Boni, A., Sangregorio, C., Corrias, A., 2010. Synthesis and microstructure of manganese ferrite colloidal nanocrystals. Phys. Chem. Chem. Phys. 12, 5074–508.

Granata, G., Pagnanelli, F., Moscardini, E., Takacova, Z., Havlik, T., Toro, L., 2012. Simultaneous recycling of nickel metal F. hydride, lithium ion and primary lithium batteries: Accomplishment of European Guidelines by optimizing mechanical pre-treatment and solvent extraction operations. J. Power. Sources. 212, 205-211

Duan, X., Yang, J., Gao, H., Ma, J., Jiao, L., Zheng W., 2012. Controllable hydrothermal synthesis of manganese dioxide nanostructures: shape evolution, growth mechanism and electrochemical properties. CrystEngComm, 14, 4196–4204

Goldman, A., 1993. Modern Ferrite Technology, Marcel Dekker, New York,

Jiang, J.Z., Wynn, P., Mørup, S., Okad, T., Berry, F.J., 1999. Magnetic structure evolution in mechanically milled nanostructured $ZnFe_2O_4$ particles. Nanostruct. Mate. 12, 737–740

Hochepied, J.F., Bonville, P., Pileni, M.P., 2000. Nonstoichiometric zinc ferrite nanocrystals: syntheses and unusual magnetic properties. J. Phys. Chem. B. 104, 905–912

Hu, Q., Liu Y., Gu, X., Zhao, Y., 2017. Adsorption behavior and mechanism of different arsenic species on mesoporous $MnFe_2O_4$ magnetic nanoparticles, Chemosphere. 181, 328-336.

Kale, A., Gubbala, S., Misra, R.D.K., 2004. Magnetic behavior of nanocrystalline nickel ferrite synthesized by the reverse micelle technique. J. Magn. Magn. Mater. 277, 350–358.

Naseri, M.G., Saion, E.B., Shaar, A.H., 2012. Role of PVP on the Phase Composition and Morphology of Manganese Ferrite Nanoparticles Prepared by Thermal Treatment Method, 2nd International Conference on Environment Science and Biotechnology Singapore, 48.

Naseri, M.G., Saion, E.B., Ahangar, H.A., Hashim, M., Shaar, A.H., 2011. Synthesis and characterization of manganese ferrite nanoparticles by thermal treatment method. J. Magn. Magn. Mater. 323, 1745–1749.

Pagnanelli, F., Moscardini E., Altimari P., Toro L., 2016. Cobalt products from real waste fractions of end of life lithium ion batteries. Waste. Manage. 51, 214–221.

Rao, S. R. 2006. Resource Recovery and Recycling from Metallurgical Wastes, Elsevier, ISBN 0-08-045131-4, Amsterdam

Rashad, M.M., Mohamed, M., Ibrahim, M.A., Ismail, L.F.M., Abdel-Aal, E.A., 2012. Magnetic and catalytic properties of cubic copper ferrite nanopowders synthesized from secondary resources. Adv. Powder. Technol. 23, 315-323.

Sezgin, N., Sahin, M., Yalcın, A., Koseoglu, Y., 2013. Synthesis, Characterization and, the Heavy Metal Removal Efficiency of $MnFe_2O_4$ (M=Ni, Cu) Nanoparticles. Ekoloji. 22,89-96.

Sharma, U.S., Sharma, R.N., Shah, R., 2014. Physical and Magnetic Properties of Manganese Ferrite Nanoparticles. Int. J. Eng. Res. Appl. 4, 14-17.

Shenoy S.D., Joy P.A., Anantharaman, M.R., 2004. Effect of mechanical milling on the structural, magnetic and dielectric properties of coprecipitated ultrafine zinc ferrite. J. Magn. Magn. Mater. 269, 217– 226.

Stoia, M., Muntean, C., Militaru, B., 2015. Fine $MnFe_2O_4$ nanoparticles for potential environmental applications Synthesis and characterization. J. Therm. Anal. Calorim. 121, 1003–1010.

Xia, S., Xu, X., Xu, C., Wang, H., Zhang, X., Liu, G., 2016. Preparation, characterization, and phosphate removal and recovery of magnetic $MnFe_2O_4$ nano-particles as adsorbents. Environ. Tech., 37,795-804.

Vijaya, J.J., Sekaran, G., Bououdina, M. 2015. Effect of Cu^{2+} doping on structural, morphological, optical and magnetic properties of $MnFe_2O_4$ particles/sheets/flakes-like nanostructures. Ceram. Int. 41, 15–26.

Yenial, Ü., Atia, T.A., Bulut, G., Pagnanelli, F., 2016. Synthesis of Magnetic Nanoparticles from Mining Wastes. International Mineral Processing Symposium (IMPS XV.) Istanbul, Turkey 1293-1307.

Zipare, K., Dhumal, J., Bandgar, S., Mathe, V., Shahane, G., 2015. Superparamagnetic Manganese Ferrite Nanoparticles: Synthesis and Magnetic Properties. Journal of Nanoscience and Nanoengineering 1, 178-182.

Zhang, D.E., Zhang, X.J., Ni, X.M., Zheng, H.G., Yang, D.D., 2005. Synthesis and characterization of NiFe2O4 magnetic nanorods via PEG-assisted route. J. Magn. Magn. Mater. 292, 79-82.

Zhang, S., Niu, H., Cai, Y., Zhao, X., Shi, Y., 2010. Arsenite and arsenate adsorption on coprecipitated bimetal oxide magnetic nanomaterials: $MnFe_2O_4$ and $CoFe_2O_4$, Chem. Eng. J. 158,599–607

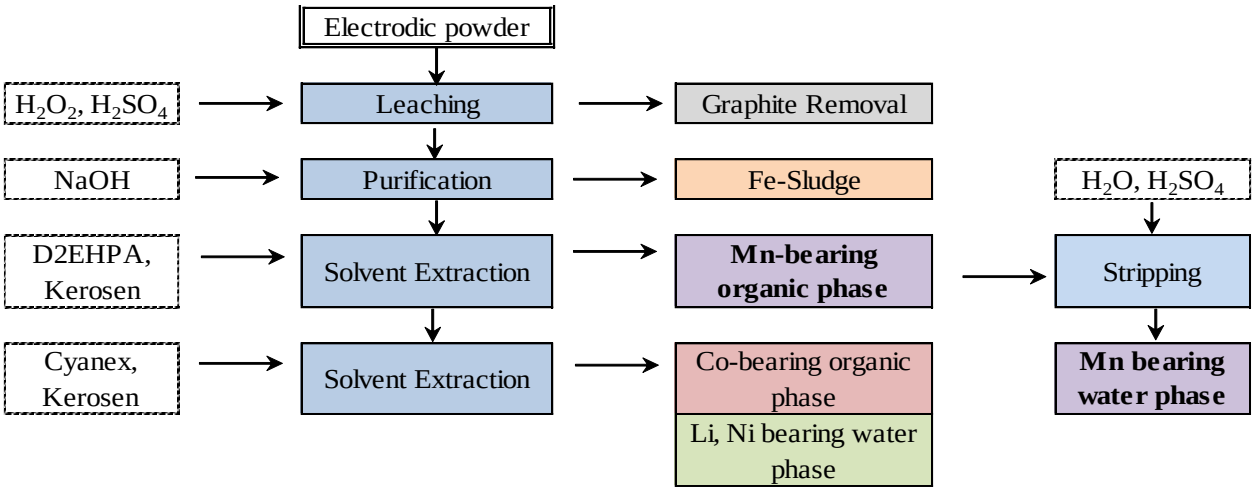

Figure 1. Flowsheet of Mn-bearing solution recovery from lithium ion batteries.

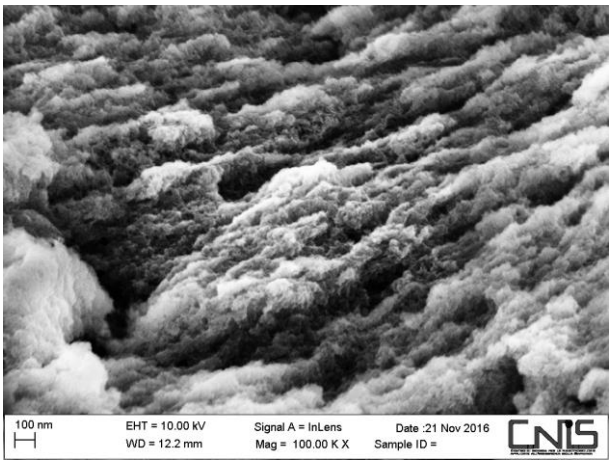

Figure 2. SEM image of sample without microwave energy (S1)

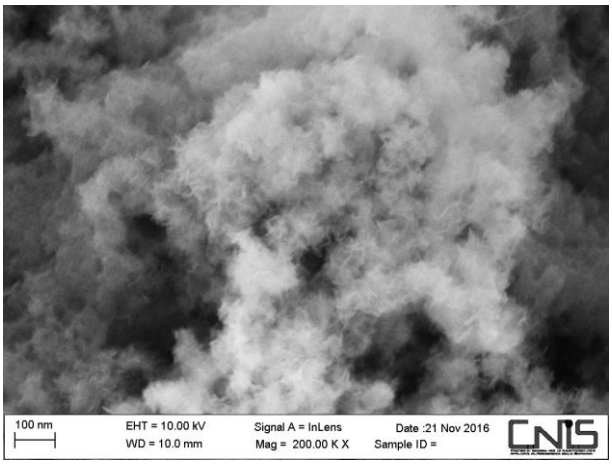

Figure 3. SEM image of sample without PVP (S2)

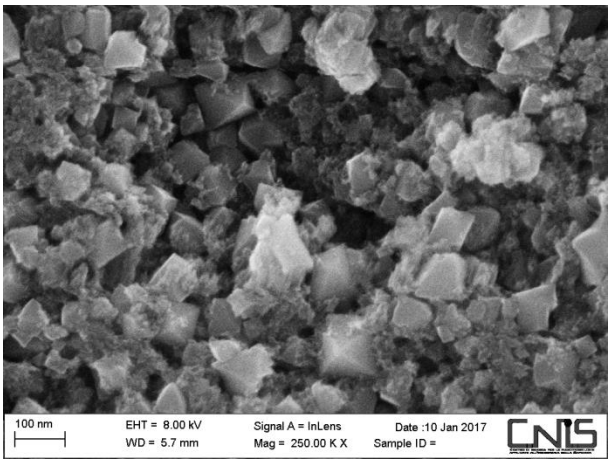

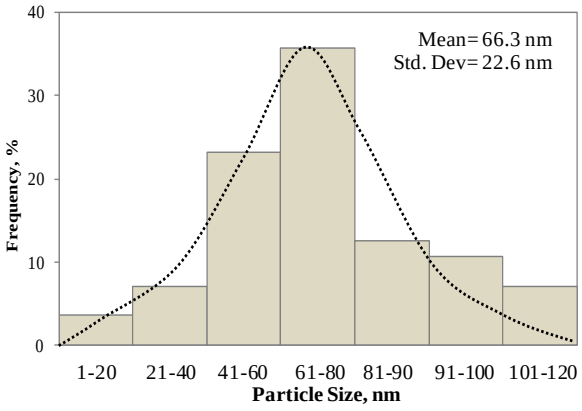

Figure 4a. SEM image of sample at 1:0.5 Fe:PVP ratio (S3) Figure 4b. Particle size distribution

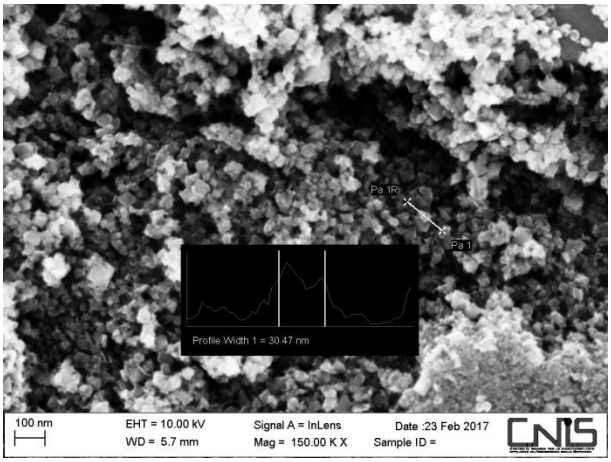

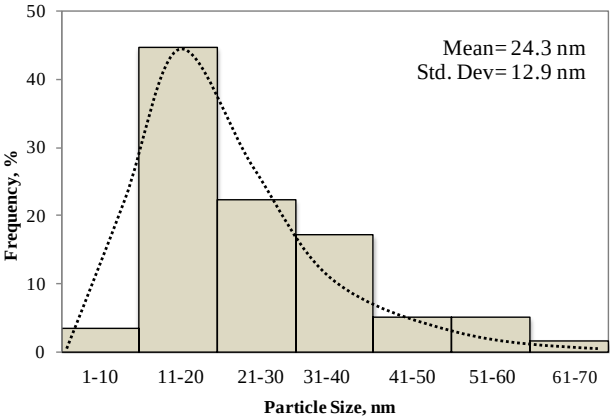

Figure 5 a: SEM image of sample at 1:1 Fe:PVP ratio (S4) Figure 5b: Particle size distribution

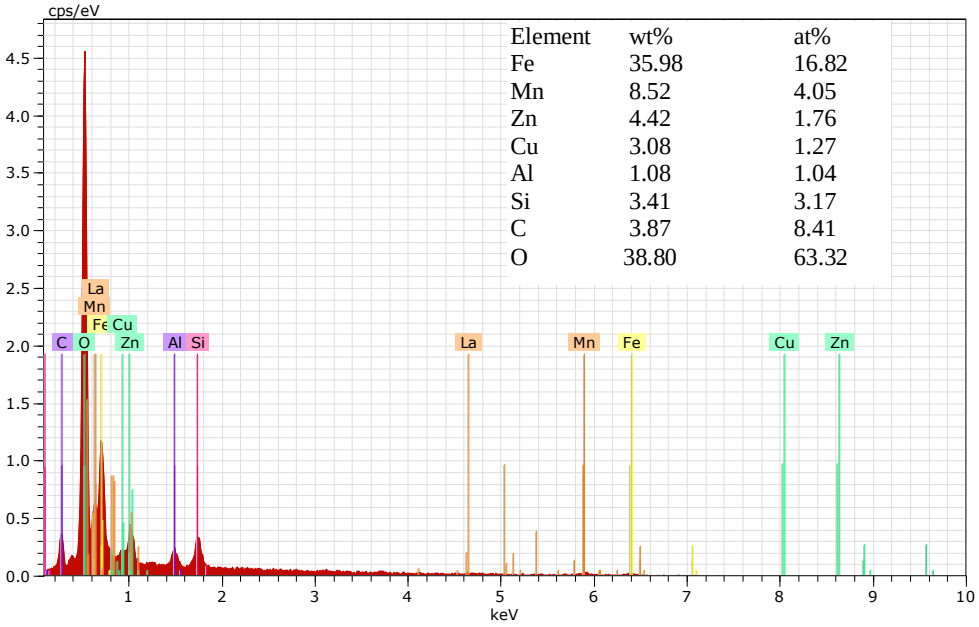

Figure 6. EDX spectra of $MnFe_2O_4$

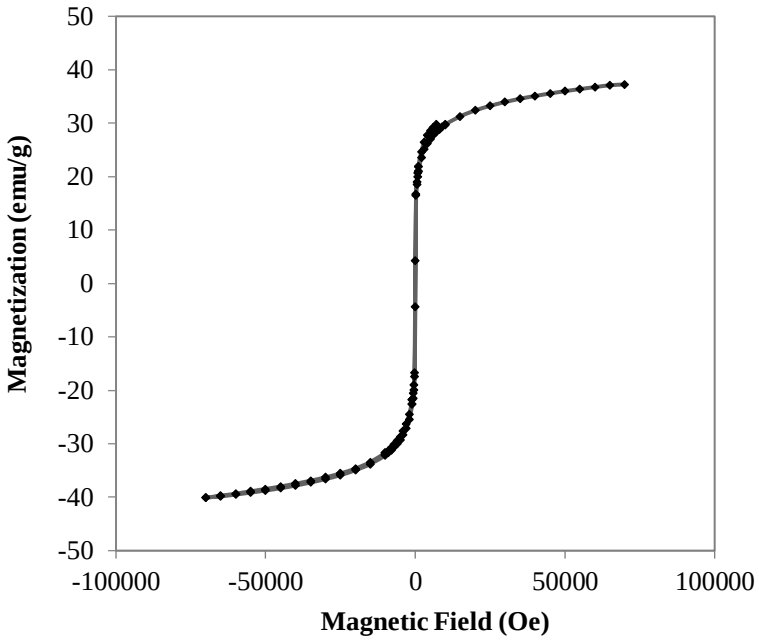

Figure 7. Hysteresis curve of manganese ferrite nanoparticles

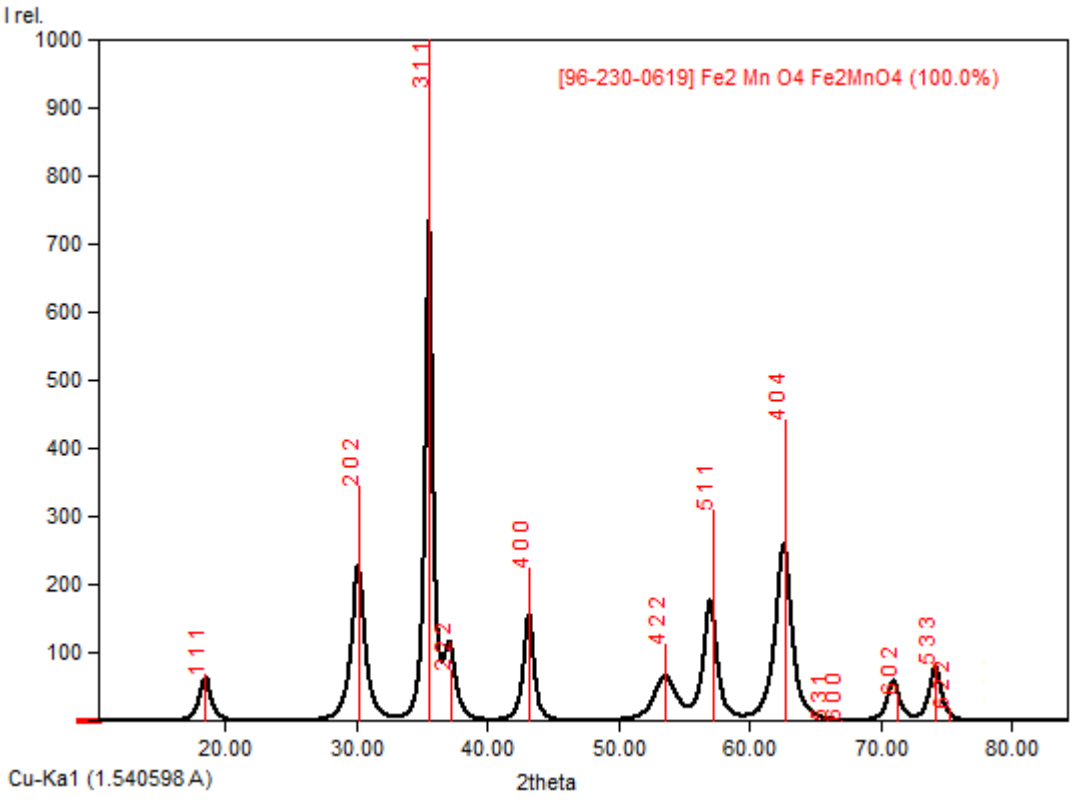

Figure 8. XRD analysis of Mn-ferrite nanoparticles

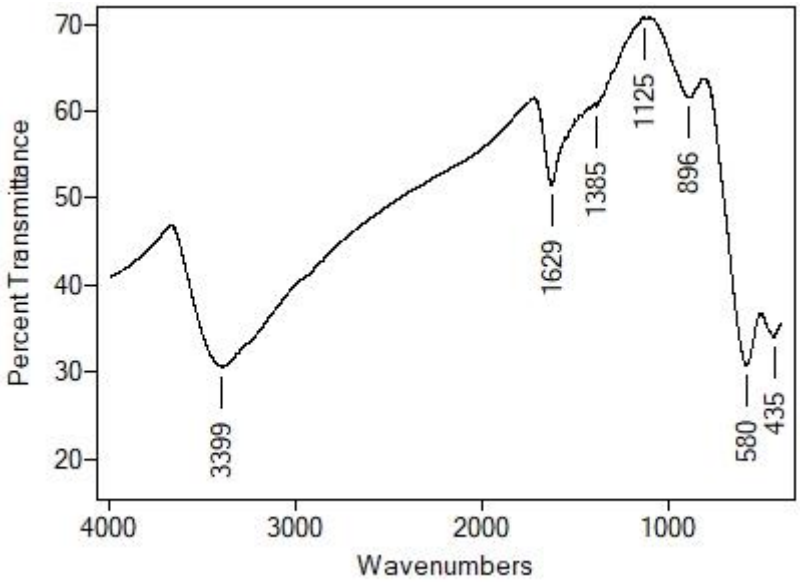

Figure 9. FT-IR analysis of $MnFe_2O_4$ nanoparticles

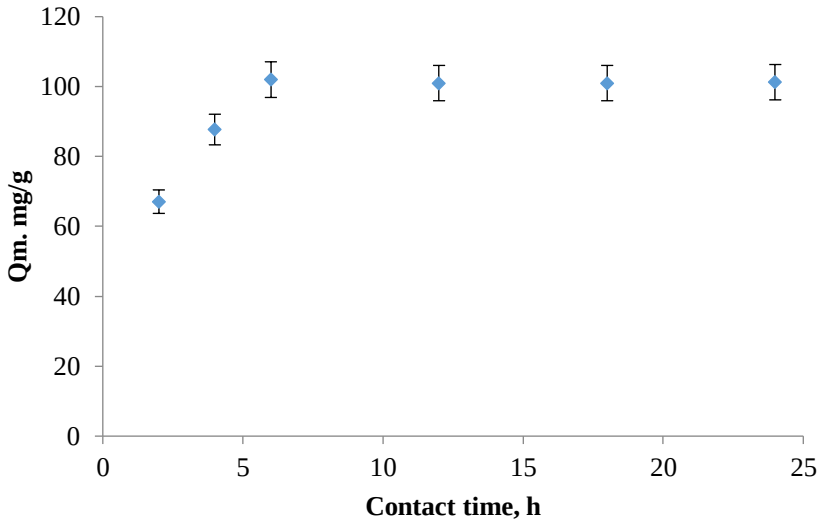

Figure 10. Effect of contact time on arsenic adsorption (the error bars correspond to variability of indicated data)

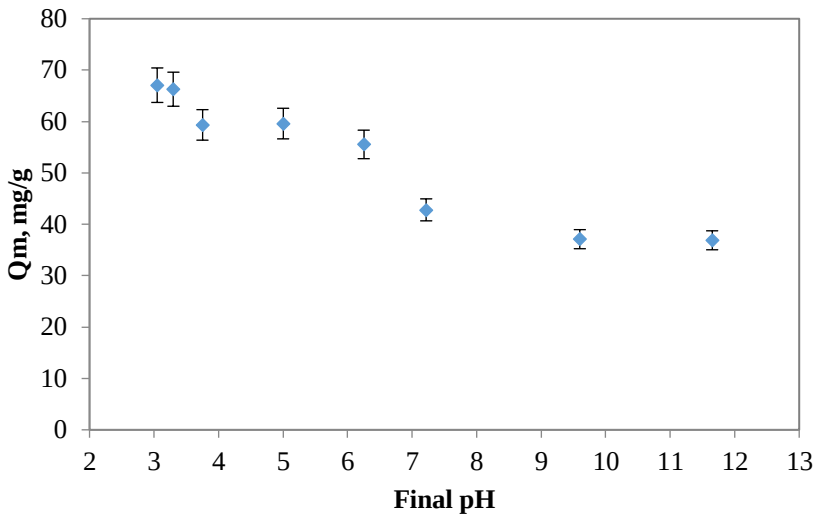

Figure 11. Effect of pH on arsenic adsorption to Mn-ferrite nanoparticles (the error bars correspond to variability of indicated data)

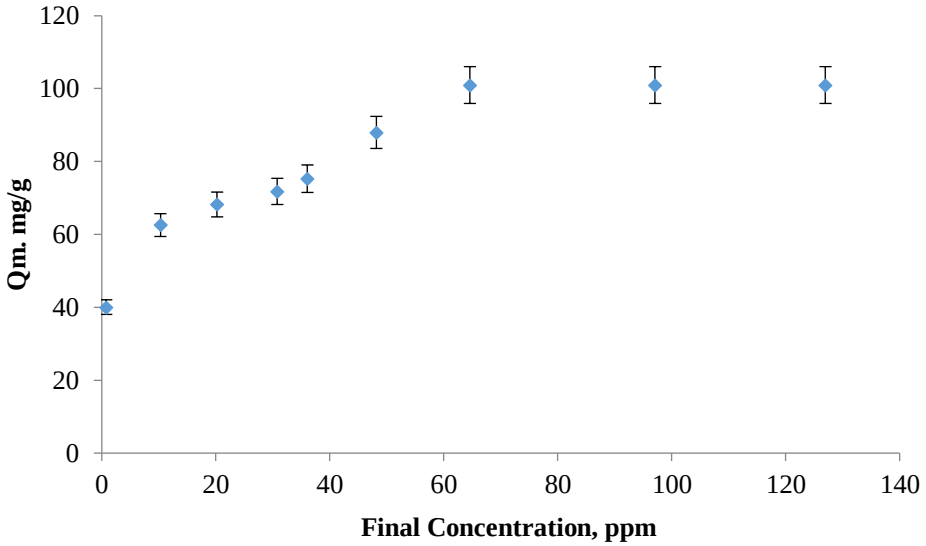

Figure 12. Experimental results of equilibrium adsorption tests. (the error bars correspond to variability of indicated data)

Table 1. The chemical analysis of leaching solutions

Fe-Leaching Solution		Mn-Stripping Solution	
Content	Concentration, g/L	Content	Concentration, g/L
Fe	10.515	Mn	1.45
Ca	0.042	Co	0.15
Cu	0.087	Cu	0.11
Zn	0.034	Ni	0.02
Al	0.003	Al	0.32

Table 2: Experimental conditions

Sample	Fe, mMol	Mn, mMol	PVP, mMol	Heat Treatment	Average Particle Sizes
S1	0.737	0.264	0.737	Dried in Oven, 24h 105°C	Undefined
S2	0.737	0.264	-	Microwave, 2h 200°C	Undefined
S3	0.737	0.264	0.368	Microwave, 2h 200°C	66.3 nm
S4	0.737	0.264	0.737	Microwave, 2h 200°C	24.2 nm

Table 3: Dissolution test of Mn-ferrite nanoparticles

pHi	pHf	Cu, %	Zn, %	Fe, %	Mn, %
2.0	1.9	22.4	13.6	0.7	36.7
3.0	3.2	13.3	6.7	udl	29.6
4.1	4.7	udl	udl	udl	2.0
5.6	5.6	udl	udl	udl	udl
7.1	7.8	udl	udl	udl	udl

*udl= under detection limit, pHi: initial pH, pHf: Final pH